2011

Experimental Validation of a Fundamental Model for PCR Efficiency

Tobias M. Louw
University of Nebraska-Lincoln

Christine S. Booth
University of Nebraska-Lincoln, christine.b2@gmail.com

Elsje Pienaar
University of Nebraska-Lincoln

Joel R. TerMaat
University of Nebraska-Lincoln, jtermaat@nebrwesleyan.edu

Scott E. Whitney
University of Nebraska-Lincoln

See next page for additional authors

Published in final edited form as:
Chem Eng Sci. 2011 April 15; 66(8): 1783–1789. doi:10.1016/j.ces.2011.01.029.
Published by Elsevier Ltd.

Experimental Validation of a Fundamental Model for PCR Efficiency

Tobias M. Louw, **Christine S. Booth**, **Elsje Pienaar**, **Joel R. TerMaat**, **Scott E. Whitney**, and **Hendrik J. Viljoen**[♣]
Department of Chemical and Biomolecular Engineering, University of Nebraska-Lincoln, Lincoln, NE 68588-0643

Abstract

Recently a theoretical analysis of PCR efficiency has been published by Booth et al., (2010). The PCR yield is the product of three efficiencies: (i) the annealing efficiency is the fraction of templates that form binary complexes with primers during annealing, (ii)the polymerase binding efficiency is the fraction of binary complexes that bind to polymerase to form ternary complexes and (iii)the elongation efficiency is the fraction of ternary complexes that extend fully. Yield is controlled by the smallest of the three efficiencies and control could shift from one type of efficiency to another over the course of a PCR experiment. Experiments have been designed that are specifically controlled by each one of the efficiencies and the results are consistent with the mathematical model. The experimental data has also been used to quantify six key parameters of the theoretical model. An important application of the fully characterized model is to calculate initial template concentration from real-time PCR data. Given the PCR protocol, the midpoint cycle number (where the template concentration is half that of the final concentration) can be theoretically determined and graphed for a variety of initial DNA concentrations. Real-time results can be used to calculate the midpoint cycle number and consequently the initial DNA concentration, using this graph. The application becomes particularly simple if a conservative PCR protocol is followed where only the annealing efficiency is controlling.

Keywords

Biological and biomolecular engineering; Enzyme; Kinetics; Mathematical modeling; Molecular biology; PCR Efficiency

1. Introduction

The polymerase chain reaction (PCR) has become a major technology in microbiology, molecular biology and related fields. Whereas PCR still has a lot of qualitative applications, it is increasingly used as a quantitative tool. The sensitivity of PCR permits amplification from a small number of starting templates. However, the exponential increase in product makes the inverse problem difficult – i.e. to infer the starting concentration from a large number of amplicons. Real-time PCR provides a proportional measure of the number of templates at each cycle.

Several methods have been proposed to calculate the initial template concentration from the real-time curves. Traditionally, standard calibration curves were used (Higuchi et al., 1993) to compare real-time results to reference samples, but this technique requires DNA standard

[♣]Author of correspondence: hviljoen1@unl.edu; (402)-472-9318 (phone); (402)-472-6989 (fax).

plasmids. Samples with known DNA concentrations are used to construct linear functions relating the initial DNA concentration to some crossover cycle number. While these functions generally correlate extremely well to experimental data, they are purely empirical in nature.

More recently, investigations of the plateau phase of the real-time PCR curve have revealed methods to calibrate the measurements “internally”, using the initial primer or probe concentrations (Swillens et al., 2004). These methods rely on mathematical models to determine the ratio between the primer-and DNA-concentrations (Smith et al., 2007). These models are usually formulated in terms of cycle efficiency.

The DNA yield depends on the efficiency of the reaction during each cycle (Saiki et al., 1985). The cycle efficiency is the product of the individual efficiencies of the denaturing, annealing, polymerase binding and elongation steps (Booth et al. 2010). As the reaction progresses the efficiency decreases resulting in the characteristic sigmoidal real-time curve (Kainz, 2000; Schnell, 1997; Schnell and Mendoza, 1997; Stolovitzky and Cecchi, 1996).

Numerous mathematical models of varying complexity have been published describing the reaction. The most general models assume constant efficiencies across all of the PCR cycles: the $\Delta\Delta C_T$ method assumes 100% efficiency while methods by Pfaffl (2001) and Liu and Saint (2002a) calculate reaction specific efficiencies. When these methods are applied for quantitative real-time PCR, they are only applied to the early phase of the reaction when efficiency is assumed to be nearly constant. More complex models account for per cycle variation in efficiency, but still combine the efficiencies of each step (denaturing, annealing and elongation) into an overall efficiency for each cycle (Liu and Saint 2002b, Platts et al., 2008). While some models account for the decrease in cycle efficiency using empirical estimates (Alvarez et al., 2007), even more complex models consider the efficiency of the steps of each cycle independently, but require numerical solution, making them difficult to apply (Gevertz et al., 2005; Mehra and Hu, 2005; Rubin and Levy, 1996; Smith et al. 2007).

The mathematical model described in Booth et al.(2010) presents an analytical model that can be used to better understand the PCR process. The model provides explicit expressions for the efficiencies of each individual PCR cycle. These efficiencies are combined into an easily implementable expression for the yield per cycle.

The model shows that different mechanisms may control the efficiency. A decrease in polymerase concentration and/or elongation time reduce the cycle efficiency, but do not affect the final template concentration (the sigmoidal concentration curve shifts laterally). Decreasing the primer concentration not only decreases the efficiency, but also decreases the final template concentration. Some model parameters, such as reaction rate constants, are unknown and must be determined by matching the model with experimental results. A short review of the model and the key parameters is given in the next section.

Experimental validation of the mathematical model presented by Booth et al., (2010) is presented in this work. Various real-time experiments have been designed to explore reactions that are limited by the annealing-, polymerase binding-and elongation efficiencies. These results have been used to determine the unknown model parameters. Finally, it is shown that this model provides an elegant method to determine initial DNA concentrations, using real-time data and the PCR protocol.

2. Mathematical Model

An analytical model was used to calculate the template concentration S_j for each PCR cycle j. The template is the region of the sample DNA flanked by the sense-and anti-sense primers

for replication; thus the initial DNA concentration is equal to the initial template concentration. For a complete derivation of the model, see Booth et al. (2010). The model is based on the following assumptions:

- There are equal numbers of forward and reverse primers and they anneal to equal numbers of sense and anti-sense single stranded DNA.
- All of the double-stranded DNA denatures completely to form single-stranded DNA.
- No primer-dimers are formed, nor does non-specific primer-template annealing occur.
- Primer-template annealing does not occur during the elongation phase.
- The annealing and elongation reactions are irreversible at the relevant temperatures.
- Partial elongation is not considered. Strands that are not fully extended by the end of the elongation cycle are treated as primers in subsequent cycles.
- The extension rate remains constant, i.e. no slow-down due to pyro-phosphorolysis or dNTP depletion.

The model calculates an overall per cycle efficiency (η_j), which is the product of three individual efficiencies. The annealing efficiency ($\eta_{j,a}$) is the fraction of available templates that anneal to primers. The polymerase binding efficiency ($\eta_{j,E}$) is the fraction of template-primer (binary) complexes that bind to polymerase to form ternary complexes. Finally, the elongation efficiency ($\eta_{j,e}$) is the fraction of ternary complexes that are fully extended by the end of the elongation step:

$$\eta_j=\eta_{j,a}\eta_{j,E}\eta_{j,e} \tag{1}$$

$$\eta_{j,a}=(P_j - P_{j,a})/S_j \tag{2}$$

$$\eta_{j,E}=C_{j,e}/(B_{j,a}+C_{j,a}) \tag{3}$$

$$\eta_{j,e}=C_{j,c}/C_{j,e} \tag{4}$$

The variables are defined in Table I and II. The subscript j identifies the cycle and the subscripts a and e denote values at the end of the annealing and elongation stages respectively. For example, there are S_j templates and P_j primers at the start of cycle j, but at the end of the annealing stage there are $P_{j,a}$ primers left. Thus the number of binary and ternary complexes that have formed during the annealing stage is ($P_j - P_{j,a}$) and the ratio ($P_j - P_{j,a}$)/S_j defines the annealing efficiency. Equations (5), (6) and (7) give the primer, ternary and binary complex values at the end of the annealing stage. The number of ternary complexes at the end of the elongation stage is given by eq. (8). The ternary complex concentration at the cut-off time ($C_{j,c}$) is the amount of primer-template-polymerase complexes that have formed after $t_c = t_e - l/V$ time has passed in the elongation phase. The value l/V is the time it takes the polymerase to extend the primer to full length DNA. Thus, $C_{j,C}$ is the concentration of ternary complexes that will fully extend by the end of the elongation phase. This value is calculated using eq.(8) with t_e replaced by t_C.

$$P_{j,a}=P_j\left(1+\gamma(\beta-1)(1-\exp\left(-k_p t_a P_j(\gamma(\beta-1)+1)^{\frac{1}{1-\beta}}\right)\right)^{\frac{1}{1-\beta}} \tag{5}$$

$$C_{j,a}=E_j\left(1-\frac{(P_j-P_{j,a})-E_j}{(P_j-P_{j,a})\exp\left(\left((P_j-P_{j,a})-E_j\right)k_c t_a\right)-E_j}\right) \tag{6}$$

$$B_{j,a}=P_j-P_{j,a}-C_{j,a} \tag{7}$$

$$C_{j,e}=\frac{(E_j-C_{j,a})(P_j-P_{j,a})-B_{j,a}E_j\exp\left(\left((P_j-P_{j,a})-E_j\right)k_c^* t_e\right)}{(E_j-C_{j,a})-B_{j,a}\exp\left(\left((P_j-P_{j,a})-E_j\right)k_c^* t_e\right)} \tag{8}$$

The model assumes that the double-stranded DNA denatures completely(denaturing efficiency ≈ 1). However, some templates and primers may become damaged during denaturing (Cadet et al., 2002; Hsu et al., 2004; Lindahl and Nyberg, 1972, 1974; Pienaar et al., 2006). The polymerase may also be damaged during this step (Sambrook and Russel, 2000). Taking denaturing damage into account (η_d and η_{dE} for the template and polymerase, respectively), the number of templates, primers and polymerase during each cycle can be calculated from the values at the previous cycle:

$$S_{j+1}=\eta_d(1+\eta_j)S_j \tag{9}$$

$$P_{j+1}=\eta_d(P_j-\eta_j S_j) \tag{10}$$

$$E_{j+1}=\eta_{dE}E_j \tag{11}$$

The variable S_j refers to the template concentration at the beginning of the j^{th} cycle. Therefore, the template concentration at the end of the elongation phase of cycle j is equal to S_{j+1}. This also corresponds to the $(j + 1)^{th}$ spectrometer reading, as fluorescence is measured at the end of the elongation phase. To simplify the situation, the first cycle will be counted as cycle 0. Hence, the template concentration at the end of cycle zero is given by $\mathbf{S_1}$, which corresponds to the **first** spectrometer measurement.

If the values of S_0, P_0 and E_0 are known, then the concentrations of all subsequent cycles can be calculated using eqns.(1 – 11). First, eqns.(5 – 8) are used to determine the amount of binary and ternary complexes that have formed after annealing and elongation. These concentrations are then used to determine the cycle efficiencies (eqns. 1 – 4) and the template, primer and polymerase concentrations at the beginning of the next cycle are calculated (eqns. 9 – 11). The function values S_j can be calculated – clearly quantitative PCR is an inverse problem.

The model parameters are listed in Table I. The initial conditions and PCR protocol parameters (experimental parameters) are known and fixed before the experiment. The model parameters are unknown and must be determined by matching experimental and theoretical data.

The rate of polymerase binding to form a ternary complex changes as the temperature increases from the annealing temperature to the elongation temperature. The value of $k_C^* > k_c$ reflects this increase in the polymerase binding rate.

The cycle dependent variables are listed and explained in Table II.

3. Materials and Methods

The reference PCR mixture contained 0.5U KOD Hot Start DNA polymerase (Novagen, Madison, WI). It was estimated that 0.5U KOD polymerase is equivalent to a concentration of 0.084 μM (Mamedov et al., 2008). The reference mixture also contained 1X polymerase manufacturer's buffer, 200 μM of each dNTP, 3.5mM $MgSO_4$, 400 μg/ml non-acetylated BSA and 3μM SYTO13 (Invitrogen, Carlsbad, CA). 0.3 μM of each primer was used for a 1002 bp product. PCR was performed in a PCR Jet Thermocycler (Megabase Research Products, Lincoln, NE) in 25 μl reaction volumes containing 1 ng bacteriophage λ genomic DNA (Genbank accession #NC_001416). The DNA was ordered from New England Biolabs (Ipswich, MA, part #N3011S, 250 μg in a 500 μg/ml concentration) and 1 ng of DNA in 25 μl corresponds to a concentration of 1.27 pM. Thermocycling consisted of a 30 second hot start at 96°C, 90 cycles of 2 s denaturing at 96°C, 3 s annealing at 64°C and 10 s elongation at 72°C. Real-time data was collected at the end of each elongation step.

Seven different experiments were performed to investigate the effects of the key experimental parameters. These parameters are listed in Table III. Each experiment was repeated three times and the average values were calculated. The average values were used to determine the unknown model parameters. The remaining experimental parameters were kept constant (t_a =3 s, V =300 bp/s, l =1002 bp). The polymerase extension rate V was obtained from Griep et al. (2006).

Although a rapid PCR protocol was used, there is still a finite amount of transition time between each of the three phases. To accommodate for ramp-times between the annealing and elongation phase, half a second was added to the elongation time in the mathematical model.

Three additional experiments were conducted using a conservative PCR protocol. This set of experiments was used to test a method for determining the initial template concentration S_0, as discussed in section 5. For these experiments, the annealing-and elongation-time was held constant at t_a =10 s and t_e = 20 s. Table IV lists the initial conditions for this set.

4. Results

4.1 Determination of model parameters

The model depends on six parameters (Table I). The parameters are determined by fitting the results of the model to the experimental results. In Table V the parameters that produced a least square error fit for **all** experiments are listed. The least square error parameters for each individual experiment were also calculated and used to determine the standard deviation of each parameter with respect to the best fit for all experiments. The standard deviation is also indicated in Table V. The rate constants are in accordance with Gevertz et

al., (2005), who used values of $k_P = 1\ (\mu Ms)^{-1}$ and $\beta = 1$. Furthermore, $k_c \approx k_c^*$, indicating that the polymerase annealing rate does not increase dramatically with temperature.

In Figure 1 the experimental results and the results of the mathematical model are compared for the parameters as listed in Table V.

4.2 The PCR Efficiencies

Once the parameters of the model have been determined, they can be used to calculate the different efficiencies, as given by eqns.(1– 11). The theoretical cycle efficiencies for experiments 1, 3–7 (cf. Table III) are shown in Figure 2. The parameter values of Table V and the concentrations and PCR protocol values as explained in Section 3 and Table III have been used to model the different experiments.

In Figure 2-A the efficiencies are shown for the reference experiment. The annealing efficiency is smaller than the polymerase and extension efficiencies, hence the experiment is under annealing control. This is not surprising, since the annealing time is only 3 seconds. However, the polymerase binding efficiency η_E exhibits a local minimum and maximum in the 20 to 30 cycle range. This cycle range is marked by a rapid increase in templates and concomitantly the binary complexes. Therefore the demand on polymerase to form ternary complexes increases; later, as the plateau phase is approached, fewer binary complexes form (lower demand on polymerase) and the fraction of binary complexes that convert to ternary complexes increases (an increase in polymerase efficiency). The continued decline in the polymerase efficiency during the plateau phase is primarily due to polymerase damage η_{dE}.

It can also be noted from Figure 2-A that the elongation efficiency is the highest of all three, but a small up tick is found in the cycle range that coincides with the local dip in polymerase efficiency. As explained in the previous paragraph, if the fraction of binary complexes that convert to ternary complexes decreases during the period of rapid increase in templates, then the polymerase binding efficiency will decrease ($C_{j,e}$ appears in numerator of eq.(3)) and the elongation efficiency will increase ($C_{j,e}$ appears in denominator of eq.(4)).

The efficiency profile is similar for the dilution experiments(Figure 2-B). The decrease in annealing efficiency is shifted laterally as a lower initial template concentration is used. The polymerase binding efficiency does play a more significant role – this is due to significant polymerase damage by the time η_E becomes controlling. This leads to a slight overall decrease in efficiency.

The reduced primer experiment (Figure 2-C) is especially sensitive to the rate of primers annealing(k_P), as this experiment is strongly controlled by annealing efficiency. When the initial primer concentration is increased (Figure 2-D), the polymerase binding efficiency becomes controlling during the exponential growth period (cycles 20 to 30) as the ratio between available polymerase and binary complexes decreases. The polymerase efficiency plays a much more controlling role when the polymerase concentration is lowered, as shown in Figure 2-E. Here, the annealing efficiency is only controlling during the initial cycles of the process. After cycle 20, the efficiency is under polymerase binding control. Figure 2-F shows the results for an experiment with reduced elongation times. The elongation efficiency is controlling for the first 30 cycles, then the system is controlled by polymerase binding for the duration of the process.

The overall efficiency in the reduced polymerase and short elongation time experiments decreases gradually, as opposed to the sudden decrease found in the reactions that are purely annealing limited. Compare the overall efficiencies at cycle 40 in Figures 2-A, 2-C and 2-D with the values in Figures 2-E and 2-F. If the system is under polymerase or elongation

control, then the template concentration is no longer symmetrical around the inflection point (typical sigmoidal shape), but a slow decrease in the slope after the inflection point occurs (compare respective experimental curves in Figure 1-C, D). These experimental results are consistent with the mathematical model (cf. Conclusions section of Booth *et al*. (2010)).

4.3 Quantitative PCR Application

In Figure 1 the model (eqns. (1–11)) has been fitted to the experimental results to determine the parameters – the best fit values are listed in Table V. Of particular importance is β =1 (signifying the competition between primer-template and template-template annealing) since it changes eq.(5) qualitatively. By taking the limit $\beta \rightarrow 1$, eq. (5) is written in the simpler form:

$$P_{j,a}=P_j \exp\left(-\gamma_j(1-\exp(-k_p t_a P_j \exp(-\gamma_j)))\right) \tag{12}$$

The model, which now comprises of eqns. (1–4), (6–12), can be used to solve the inverse problem, i.e. determining the initial template concentration (S_0). If a value for S_0 is guessed, the model can be solved and the resulting curve S_j vs. j can be compared to the experimental curve (on a normalized basis) until a best fit is obtained. This approach is cumbersome.

A simpler procedure is devised by using the midpoint cycle number, which is defined as the cycle that corresponds to half the plateau (or maximum) value: S_M =max(S_j)/2. The mid-point cycle number M is uniquely determined by S_0 and the PCR conditions. The locus of M as a function of S_0 can be determined using the mathematical model and the graph of M vs. $\log_2(P_0/S_0)$ can be constructed. This is shown in Figure 3-B. Determining the initial template concentration becomes straightforward: the midpoint cycle number M is determined from the experimental real time results. This value is used to determine $\log_2(P_0/S_0)$ from the graph(constructed using the mathematical model, as above). Finally, this can be used to calculate S_0 as P_0 is known.

4.3.1 Conservative elongation time—The calculation of the midpoint cycle number locus can be further simplified if the PCR conditions are chosen conservatively. For example, if the elongation times are long with respect to the minimum elongation time l/V, then the effect of the elongation efficiency becomes negligible (i.e. $\eta_e \approx 1$). For our template length and choice of polymerase this conservative protocol is achieved by setting the elongation time equal to 20 seconds (longer templates/polymerases with slower elongation rates will require longer elongation times). The model reduces to three equations, given by eqns. (12–14). Note that annealing time and initial polymerase concentration are still present in the model.

$$S_{j+1}=S_j+\min(P_j-P_{j,a},\ \eta_{dE}^j E_0) \tag{13}$$

$$P_{j+1}=P_j-\min(P_j-P_{j,a},\ \eta_{dE}^j E_0) \tag{14}$$

Remark: Equation 13 implies that if the amount of available polymerase ($E_j=\eta_{dE}^j E_0$) is greater than the amount of primer-template complexes ($P_j - P_{j,a}$), then the amount of new templates formed is equal to the amount of binary complexes formed. If $\eta_{dE}^j E_0 < P_j - P_{j,a}$, then the reaction is limited by the amount of polymerase available.

The locus M vs. $\log_2(P_0/S_0)$ can be calculated using eqns. (12–14) for a conservative elongation time protocol. Application remains the same; the midpoint cycle number is determined from the real time data and used to determine $\log_2(P_0/S_0)$ from the locus. This is shown in Figure 3-B.

4.3.2 Conservative elongation time and excess polymerase—If the experiment is setup so that $\eta_{dE}^{j} E_0 > P_j - P_{j,a}$ for all cycles j, then a further simplification can be made:

$$S_{j+1} = S_j + P_j - P_{j,a} \tag{15}$$

$$P_{j+1} = P_{j,a} = P_j \exp\left(-\gamma_j (1 - \exp(-k_p t_a P_j \exp(-\gamma_j)))\right) \tag{16}$$

4.3.3 Conservative elongation and annealing times and excess polymerase— Finally, one can use conservative annealing times to arrive at the model:

$$S_{j+1} = S_j + P_j - P_{j,a} \tag{17}$$

$$P_{j+1} = P_{j,a} = P_j \exp(-\gamma_j) \tag{18}$$

In eqns.(17–18), the only factor that limits templates from doubling at each cycle is the competition between single stranded DNA to bind to complementary strands instead of primers. It is interesting to note that during the early stages of the experiment, when the primers are in excess and $\gamma_j = S_j/P_j$ is small, the exponential term in eq.(18) is well approximated by a linear expansion. If a linear expansion is used, then eq.(17) leads to the following well-known result:

$$S_{j+1} = S_j + P_j - P_j \exp\left(-\frac{S_j}{P_j}\right) \approx S_j + P_j - P_j\left(1 - \frac{S_j}{P_j}\right) = 2S_j \tag{19}$$

Equations(17–18) presents the most ideal case, but it is important to see that all the conservative protocols are only simplifications of the general model. Thence a quantitative analysis can be done for any set of PCR conditions.

The experiments listed in Table IV correspond to a conservative elongation time protocol – i.e. eqns.(12–14). Figure 3-A shows the spectrometer readings compared to the simplified model. It is clear that a change in initial template concentration produces a lateral shift in the real-time curve. The mid-point value for each experiment is indicated with a grey cross on Figure 3-A. In Figure 3-B we plot the locus of M vs. $\log_2(P_0/S_0)$ -shown as the dashed line. The three experimental values of M are also marked on the locus. Suppose the initial concentrations were not known, then the experimentally obtained values of M (Figure 3-A) would be used to read off $\log_2(P_0/S_0)$ from the dashed line in Figure 3-B.

The fast protocol that was used for experiments listed in Table III requires that we use the general model (1–4, 6–12). The theoretically determined locus for the fast protocol is shown as the solid line in Figure 3-B. Values of M for experiments 1–3(Table III) are also plotted on the locus. Finally the locus obtained using eqns. (17–18) are plotted as the dotted line in Figure 3-B. Note that the most conservative model forms a lower bound for the other

models. It becomes quite clear how PCR conditions impact the template amplification and how to account for protocol changes quantitatively. This analysis becomes especially helpful in a time where rapid PCR is used more in point-of-care diagnosis applications.

6. Conclusions

The fundamental, analytical model presented by Booth et al. (2010) was investigated and the following was found:

- The model matches experimental results and exposes the underlying factors driving the polymerase chain reaction;
- Model parameters were determined (Table V) that can be used in future experiments. Some variation is possible for the values of K_c, k_c^* and η_{dE} when different polymerases are used. It is expected that K_p and β will remain constant for many different experiments;
- Using the model parameters, the full mathematical model was simplified to one that could easily be implemented if a conservative PCR protocol was used
- Using model predictions, many PCR reactions can be simulated to find the optimal PCR protocol. This will allow increased throughput of PCR assays;
- Functions relating the initial DNA concentration to the midpoint cycle number (similar to those first implemented by Higuchi et al., 1993) were created on a fundamental basis, and found to correlate well with experimental data. This can be used to quantify the initial amount of DNA in a sample.
- The method of quantifying initial DNA concentration can be applied to rapid PCR protocols as well, which is extremely important in point-of-care diagnostic applications.

The research conducted here provides a theoretical basis for the optimization of PCR and the quantitative analysis of real-time data.

Acknowledgments

Financial support for this work has been provided through a grant by the National Institutes of Health (1R33RR022860-03).

References

Alvarez MJ, Vila-Ortiz G, Salibe MC, Podhajcer OL, Pitossi FJ. Model based analysis of real-time PCR data from DNA binding dye protocols. BMC Bioinformatics. 2007; 8(85)

Booth CS, Pienaar E, TerMaat JR, Whitney SE, Louw TM, Viljoen HJ. Efficiency of the polymerase chain reaction. Chemical Engineering Science. 2010; 65(17):4996–5006. [PubMed: 21799540]

Cadet J, Bellon S, Berger M, Bourdat A, Douki T, Duarte V, Frelon S, Gasparutto D, Muller E, Ravanat J, Sauvaigo S. Recent aspects of oxidative DNA damage: guanine lesions, measurement and substrate specificity of DNA repair glycosylases. Biological chemistry. 2002; 383(6):933–43. [PubMed: 12222683]

Gevertz JL, Dunn SM, Roth CM. Mathematical Model of Real-Time PCR Kinetics. Biotechnology and bioengineering. 2005; 92(3):346–355. [PubMed: 16170827]

Griep M, Kotera C, Nelson R, Viljoen H. Kinetics of the DNA polymerase pyrococcus kodakaraensis. Chemical Engineering Science. 2006; 61(12):3885–3892.

Higuchi R, Fockler C, Dollinger G, Watson R. Kinetic PCR analysis: real-time monitoring of DNA amplification reactions. Nature Biotechnology. 1993; 11(9):1026–1030.

Hsu GW, Ober M, Carell T, Beese LS. Error-prone replication of oxidatively damaged DNA by a high-fidelity DNA polymerase. Nature. 2004; 431(7005):217–221. [PubMed: 15322558]

Kainz P. The PCR plateau phase-towards an understanding of its limitations. Biochimica et Biophysica Acta (BBA)-Gene Structure and Expression. 2000; 1494(1–2):23–27.

Lindahl T, Nyberg B. Heat-induced deamination of cytosine residues in deoxyribonucleic acid. Biochemistry. 1974; 13(16):3405–3410. [PubMed: 4601435]

Lindahl T, Nyberg B. Rate of depurination of native deoxyribonucleic acid. Biochemistry. 1972; 11(19):3610–3618. [PubMed: 4626532]

Liu W, Saint DA. A new quantitative method of real time reverse transcription polymerase chain reaction assay based on simulation of polymerase chain reaction kinetics. Analytical Biochemistry. 2002a; 302(1):52–59. [PubMed: 11846375]

Liu W, Saint DA. Validation of a quantitative method for real time PCR kinetics. Biochemical and biophysical research communications. 2002b; 294(2):347–353. [PubMed: 12051718]

Mamedov TG, Pienaar E, Whitney SE, TerMaat JR, Carvill G, Goliath R, Subramanian A, Viljoen HJ. A fundamental study of the PCR amplification of GC-rich DNA templates. Computational biology and chemistry. 2008; 32(6):452–7. [PubMed: 18760969]

Mehra S, Hu W. A Kinetic Model of Quantitative Real-Time Polymerase Chain Reaction. Biotechnology and bioengineering. 2005; 91(7):848–860. [PubMed: 15986490]

Pfaffl MW. A new mathematical model for relative quantification in real-time RT-PCR. Nucleic acids research. 2001; 29(9):e45. [PubMed: 11328886]

Pienaar E, Theron M, Nelson M, Viljoen HJ. A quantitative model of error accumulation during PCR amplification. Computational biology and. 2006; 30(2):102–111.

Platts AE, Johnson GD, Linnemann AK, Krawetz SA. Real-time PCR quantification using a variable reaction efficiency model. Analytical Biochemistry. 2008; 380(2):315–322. [PubMed: 18570886]

Rubin E, Levy AA. A mathematical model and a computerized simulation of PCR using complex templates. Nucleic acids research. 1996; 24(18):3538–3545. [PubMed: 8836180]

Saiki RK, Scharf S, Faloona F, Mullis KB, Horn GT, Erlich HA, Arnheim N. Enzymatic Amplification of -globin Genomic Sequences and Restriction Site Analysis for Diagnosis of Sickle Cell Anemia. Science. 1992; 230(4732):1350–1354. [PubMed: 2999980]

Sambrook, J.; Russel, DW. Cold Spring Harbor. New York: Cold Spring Harbor Laboratory Press; 2000. Molecular Cloning: A Laboratory Manual.

Schnell S. Enzymological Considerations for the Theoretical Description of the Quantitative Competitive Polymerase Chain Reaction (QC-PCR). Journal of theoretical biology. 1997; 184(4): 433–440. [PubMed: 9082073]

Schnell S, Mendoza C. Theoretical description of the polymerase chain reaction. Journal of theoretical biology. 1997; 188(3):313–318. [PubMed: 9344735]

Smith MV, Miller CR, Kohn M, Walker NJ, Portier CJ. Absolute estimation of initial concentrations of amplicon in a real-time RT-PCR process. BMC Bioinformatics. 2007; 8(409)

Stolovitzky G, Cecchi G. Efficiency of DNA replication in the polymerase chain reaction. Proceedings of the National Academy of Sciences of the United States of America. 1996; 93(23):12947–12952. [PubMed: 8917524]

Swillens S, Goffard JC, Maréchal Y, de Kerchove d'Exaerde A. Instant evaluation of the absolute initial number of cDNA copies from a single real-time PCR curve. Nucleic acids research. 2004; 32(6):e56. [PubMed: 15054124]

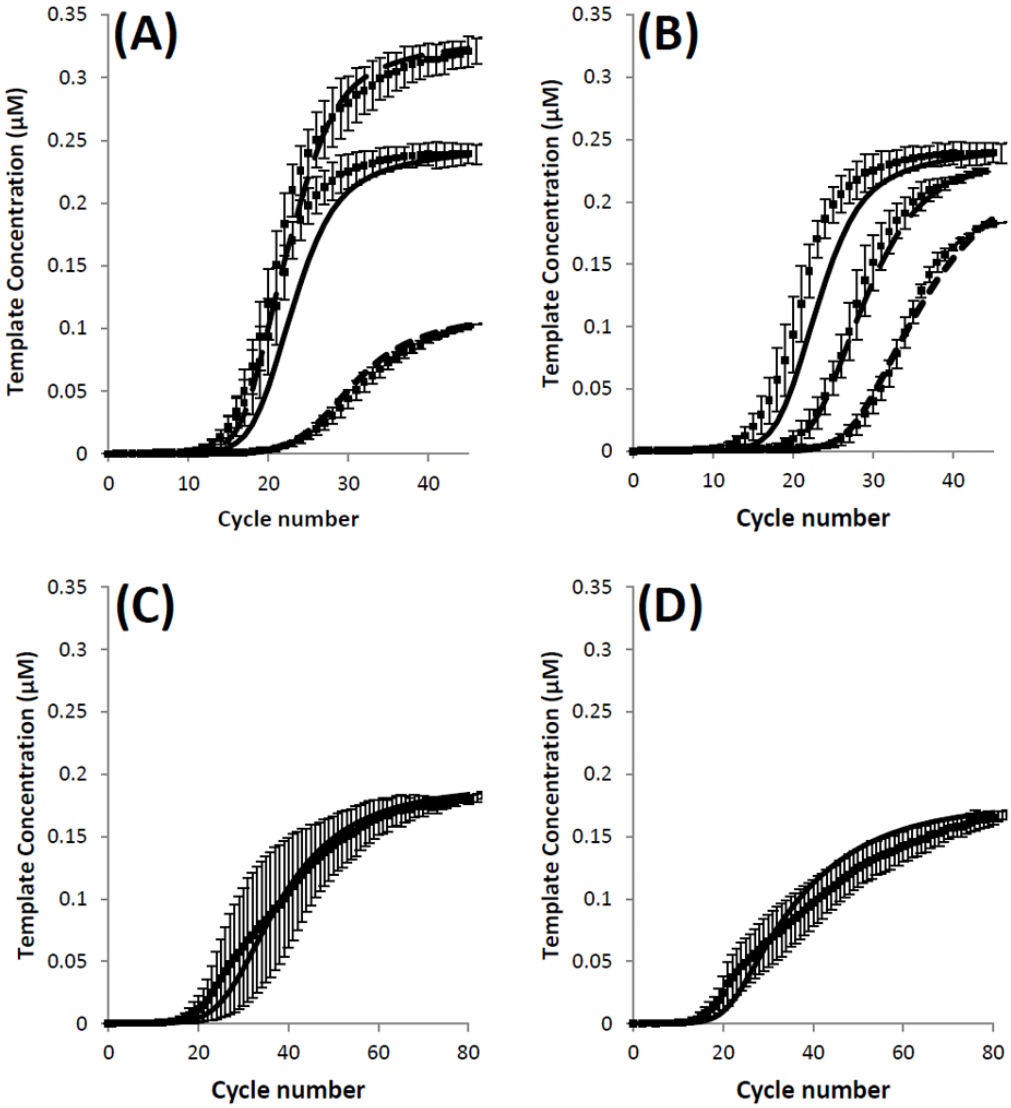

Figure 1.

Results for experiments 1–7 (with one standard deviation error bar) and the model predictions (solid lines) for parameter values listed in Table V. (A) Reference (solid line), Increased- (dashes) and reduced-primer concentration (short dashes) experiments. (B) Reference (solid line), Dilution I (dashes) and Dilution II (short dashes) experiments. (C) Short elongation time. (D) Reduced polymerase concentration.

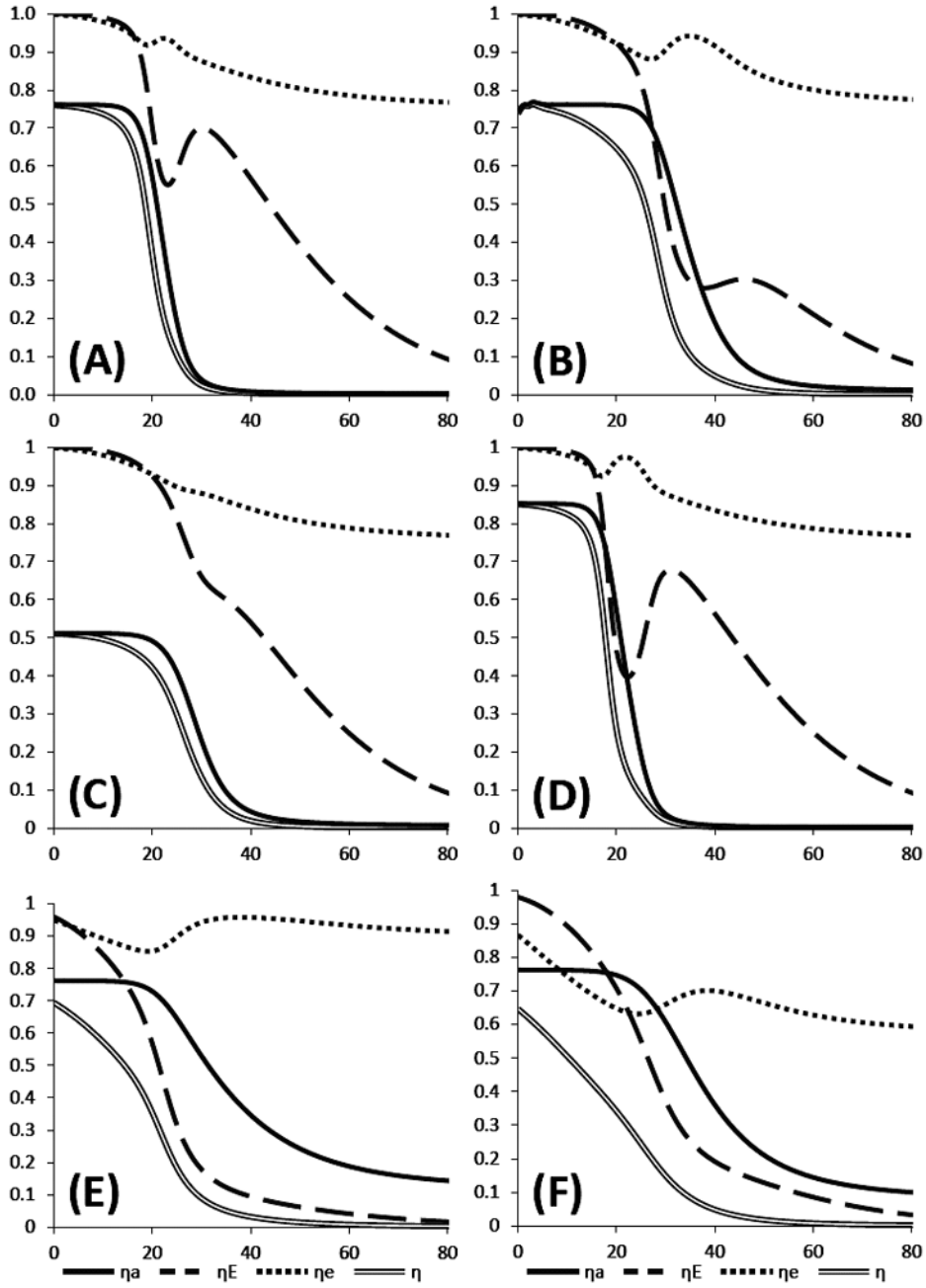

Figure 2.

The annealing (η_a), polymerase binding (η_E), elongation (η_e) and total efficiency (η) for the following experiments: (A) Reference (B) Dilution II (C) Reduced Primer (D) Increased primer (E) Reduced polymerase (F) and Short elongation time.

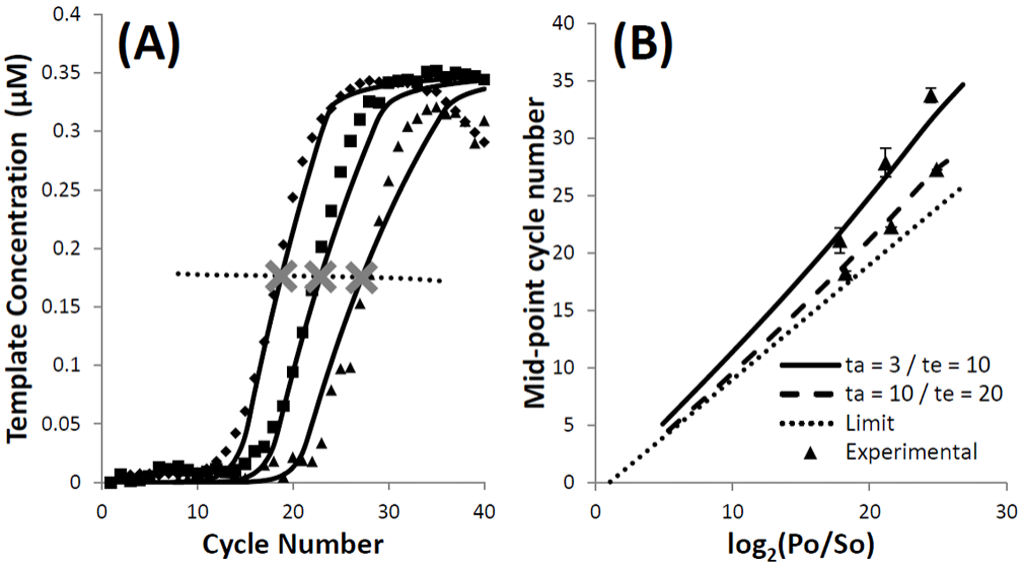

Figure 3.

(A) Results for experiments i–iii with the simplified model predictions. The dilution curves correspond to an initial template concentration of S_0 = 1.27 pM, S_0 = 0.127 pM and S_0 = 0.0127 pM. The midpoint cycle number (M) is indicated by an X. The locus of points representing M over a range of S_0 is shown by the dotted line. (B) The midpoint cycle number M as a function of $\log_2(P_0/S_0)$ for the reference (solid line) and conservative reference (dashed line) parameters, over a range of S_0 values. The actual midpoint cycle numbers obtained by fluorescent measurements are shown. As the annealing time is increased, the loci approach a limit function (dotted line).

Table I

Experimental and model parameters used in analytic model

Experimental parameters	Description	Model parameters	Description
t_a; t_e	Annealing/Elongation phase duration	k_P	Rate of primer annealing
S_0	Initial template concentration	k_C	Rate of polymerase binding at the annealing temperature
P_0	Initial primer concentration	k_C^*	Rate of polymerase binding at the elongation temperature
E_0	Initial polymerase concentration	β	Ratio of template annealing rate to primer annealing rate
V	Polymerase extension rate	η_d	Template denaturing damage
l	Template length	η_{dE}	Polymerase denaturing damage

Table II

Variables used in analytic model

Variable	Description	Variable	Description
S_j	Template concentration at the beginning of annealing	E_j	Polymerase concentration at the beginning of annealing
P_j; $P_{j,a}$	Primer concentration at the beginning and end of annealing	$B_{j,a}$	Binary complex concentration at the end of annealing
γ_j	Ratio of template to primer concentration (S_j/P_j)	$C_{j,a}$; $C_{j,e}$; $C_{j,c}$	Ternary complex concentration at the end of annealing, elongation and at the cut-off time, respectively
δ_j	Ratio of equilibrium primer concentration after annealing to S_j		

Table III

Experiments for determining model parameters (t_a = 3 s)

	Experiment	S_0 (pM)	P_0 (μM)	E_0 (units)	t_e (s)
1	*Reference*	1.27	0.30	0.5	10
2	*Dilution I*	0.127	0.30	0.5	10
3	*Dilution II*	0.0127	0.30	0.5	10
4	*Reduced primer*	1.27	0.15	0.5	10
5	*Increased primer*	1.27	0.40	0.5	10
6	*Short elongation*	1.27	0.30	0.5	3
7	*Reduced polymerase*	1.27	0.30	0.2	10

Table IV

Experiments for determining initial template concentration (t_a = 10 s, t_e = 3 s)

	Experiment	S_0 (pM)	P_0 (μM)	E_0 (units)
i	*Conservative reference*	1.27	0.4	0.5
ii	*Conservative dilution I*	0.127	0.4	0.5
iii	*Conservative dilution II*	0.0127	0.4	0.5

Table V

Physical parameters determined by matching model predictions to experimental results

k_P =1.59 ± 0.18 (μM.s)$^{-1}$	β ≈ 1
k_C =7.08 ± 0.86 (μM.s)$^{-1}$	η_d =1.00 ± 0.008
k_C^*=7.08 ± 0.86 (μM.s)$^{-1}$	η_{dE} =0.947 ± 0.005